A measurement of the neutron to ^{199}Hg magnetic moment ratio

S. Afach[a,b,c], C. A. Baker[d], G. Ban[e], G. Bison[b], K. Bodek[f], M. Burghoff[g], Z. Chowdhuri[b], M. Daum[b], M. Fertl[a,b,1], B. Franke[a,b,2], P. Geltenbort[h], K. Green[d,i], M. G. D. van der Grinten[d,i], Z. Grujic[j], P. G. Harris[i], W. Heil[k], V. Hélaine[b,e], R. Henneck[b], M. Horras[a,b], P. Iaydjiev[d,3], S. N. Ivanov[d,4], M. Kasprzak[j], Y. Kermaïdic[l], K. Kirch[a,b], A. Knecht[b], H.-C. Koch[j,k], J. Krempel[a], M. Kuźniak[b,f,5], B. Lauss[b], T. Lefort[e], Y. Lemière[e], A. Mtchedlishvili[b], O. Naviliat-Cuncic[e,6], J. M. Pendlebury[i], M. Perkowski[f], E. Pierre[b,e], F. M. Piegsa[a], G. Pignol[l], P. N. Prashanth[m], G. Quéméner[e], D. Rebreyend[l], D. Ries[b], S. Roccia[n], P. Schmidt-Wellenburg[b], A. Schnabel[g], N. Severijns[m], D. Shiers[i], K. F. Smith[i,7], J. Voigt[g], A. Weis[j], G. Wyszynski[a,f], J. Zejma[f], J. Zenner[a,b,o], G. Zsigmond[b]

[a] *ETH Zürich, Institute for Particle Physics, CH-8093 Zürich, Switzerland*
[b] *Paul Scherrer Institute (PSI), CH–5232 Villigen-PSI, Switzerland*
[c] *Hans Berger Department of Neurology, Jena University Hospital, D-07747 Jena, Germany*
[d] *Rutherford Appleton Laboratory, Chilton, Didcot, Oxon OX11 0QX, United Kingdom*
[e] *LPC Caen, ENSICAEN, Université de Caen, CNRS/IN2P3, Caen, France*
[f] *Marian Smoluchowski Institute of Physics, Jagiellonian University, 30–059 Cracow, Poland*
[g] *Physikalisch Technische Bundesanstalt, Berlin, Germany*
[h] *Institut Laue–Langevin, Grenoble, France*
[i] *Department of Physics and Astronomy, University of Sussex, Falmer, Brighton BN1 9QH, United Kingdom*
[j] *Physics Department, University of Fribourg, CH-1700 Fribourg, Switzerland*
[k] *Institut für Physik, Johannes–Gutenberg–Universität, D–55128 Mainz, Germany*
[l] *LPSC, Université Grenoble Alpes, CNRS/IN2P3, Grenoble, France*
[m] *Instituut voor Kern– en Stralingsfysica, Katholieke Universiteit Leuven, B–3001 Leuven, Belgium*
[n] *CSNSM, Université Paris Sud, CNRS/IN2P3, Orsay Campus, France*
[o] *Institut für Kernchemie, Johannes-Gutenberg-Universitat, D-55128 Mainz, Germany*

arXiv:1410.8259v2 [nucl-ex] 31 Oct 2014

Abstract

The neutron gyromagnetic ratio has been measured relative to that of the ^{199}Hg atom with an uncertainty of 0.8 ppm. We employed an apparatus where ultracold neutrons and mercury atoms are stored in the same volume and report the result $\gamma_n/\gamma_{Hg} = 3.8424574(30)$.

Keywords: ultracold neutrons, mercury atoms, magnetic moment, gyromagnetic ratio

1. Introduction

After Chadwick's discovery of the neutron in 1932, it became clear that nuclei are made out of protons and neutrons. In this picture the neutron had to bear a nonzero magnetic moment in order to account for the magnetic moments of nuclei. The observation that the neutron, an electrically neutral particle, has a nonzero magnetic moment is in conflict with the prediction of the relativistic Dirac equation valid for elementary spin 1/2 particles. This fact was an early indication of the existence of a sub-structure for neutrons and protons.

The first direct measurement of the neutron magnetic moment was reported by Alvarez and Bloch in 1940 [1] with an uncertainty of one percent. The frequency f_n of the neutron spin precession in a magnetic field B_0 was measured using the Rabi resonance method, from which the gyromagnetic ratio $\gamma_n = 2\pi f_n/B_0$ and the magnetic moment $\mu_n = \hbar/2\,\gamma_n$ were extracted. The precision of this method was then improved by using the proton magnetic resonance technique to measure the magnetic field B_0 [2, 3]. In 1956, Cohen, Corngold and Ramsey achieved an uncertainty of 25 ppm, using Ramsey's resonance technique of separated oscillating fields [4]. Then, challenged by the possible discovery of a nonzero neutron electric dipole moment (nEDM), Ramsey's technique was further developed. Profiting from these developments, Greene and coworkers [5] measured in 1977 the neutron-to-proton magnetic moment ratio with an improvement of two orders of magnitude in accuracy. In the latter experiment, the separated field resonance technique was applied simultaneously to a beam of slow neutrons and a flow of protons in water precessing in the same magnetic field.

Since 1986 the neutron gyromagnetic ratio has been considered by the Committee on Data for Science and Technology (CODATA) as a fundamental constant. In the 2010 evaluation of the fundamental constants [6], the accepted value

$$\frac{\gamma_n}{2\pi} = 29.1646943(69)\,\mathrm{MHz/T} \quad [0.24\,\mathrm{ppm}] \tag{1}$$

Email address: pignol@lpsc.in2p3.fr (G. Pignol)

[1] Now at University of Washington, Seattle WA, USA.
[2] Now at Max-Planck-Institute of Quantum Optics, Garching, Germany.
[3] On leave from INRNE, Sofia, Bulgaria.
[4] On leave from PNPI, St. Petersburg, Russia.
[5] Now at Queen's University, Kingston ON, Canada.
[6] Now at Michigan State University, East-Lansing, USA.
[7] Deceased.

was obtained by combining Greene's measurement [5] of γ_n/γ'_p with the determination of the shielded proton gyromagnetic ratio in pure water γ'_p.

In this letter we report on a measurement of the neutron magnetic moment with an accuracy of better than 1 ppm, using an apparatus that was built to search for the neutron electric dipole moment [7]. The experimental method differs in two essential aspects from the one reported in Ref. [5]. First, we use stored ultracold neutrons (UCNs) rather than a beam of cold neutrons. Second, the magnetic field is measured using a comagnetometer based on the nuclear spin precession of ^{199}Hg atoms. The result presented is, in fact, a measurement of the ratio γ_n/γ_{Hg} of the neutron to mercury ^{199}Hg magnetic moments.

Although not as suitable as the proton, the ^{199}Hg atom can also be used as a magnetic moment standard. In 1960 Cagnac measured γ_{Hg}/γ'_p in Kastler's lab using the newly invented Brossel's double resonance method [8]. Since the magnetic field was calibrated using nuclear magnetic resonance in water, the mercury magnetic moment was effectively measured in units of the proton magnetic moment. Cagnac's result $\gamma_{Hg}/\gamma'_p = 0.1782706(3)$ can be combined with the current accepted value of the shielded proton moment ($\gamma'_p/2\pi$ = 42.5763866(10) MHz/T [6]) to extract a mercury gyromagnetic ratio of

$$\frac{\gamma_{Hg}}{2\pi} = 7.590118(13)\,\text{MHz/T} \quad [1.71\ \text{ppm}]. \tag{2}$$

Our result for γ_n/γ_{Hg} with an accuracy better than 1 ppm provides an interesting consistency check on results (1) and (2). It confirms the currently accepted value of the neutron magnetic moment, which was inferred from a single experiment [5]. Alternatively, our result can be used to produce a more accurate value for the mercury magnetic moment.

2. The measurement with the nEDM spectrometer

The measurement was performed in fall 2012 with the nEDM spectrometer, currently installed at the Paul Scherrer Institute (PSI). A precursor of this room-temperature apparatus, operated at Institut Laue Langevin (ILL), has produced the currently lowest experimental limit for the neutron EDM [9]. A detailed description of the apparatus, when operated at ILL, can be found in [10]. A schematic view of the core of the apparatus, as installed now at PSI, is depicted in Fig. 1.

The spectrometer uses UCNs, neutrons with kinetic energies of $\approx$ 100 neV that can be stored in material bottles for a few minutes. In a typical measurement cycle, UCNs from the new PSI source [11] are guided to the precession chamber, filling the volume for 34 s before closing the UCN valve. The neutrons are fully polarized on their way from the source to the apparatus by a 5 T superconducting magnet. The precession chamber is a 22 liter cylindrical storage volume of height H = 12 cm made out of a deuterated polystyrene ring and two diamond-like-carbon coated flat metallic plates. The entire apparatus is evacuated to a residual pressure below 10^{-5} mbar during the measurements. After the completion of the Ramsey procedure

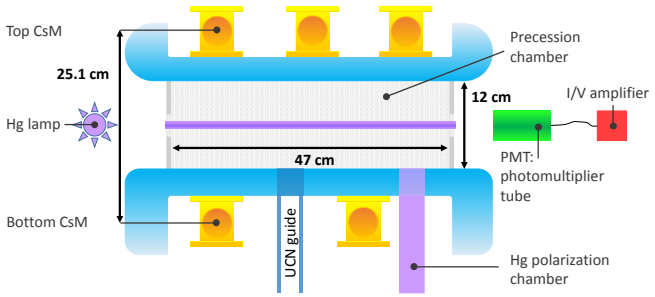


Figure 1: Vertical cut through the inner part of the nEDM apparatus. Schematically indicated are the precession chamber, the mercury comagnetometer and the Cs magnetometer array.

described below, the UCN valve is opened again and the neutrons fall down into a detector where they are counted. On the way to the detector they pass through a magnetized iron foil that serves as a spin analyzer, providing a spin-dependent counting of the neutrons.

The precession chamber is exposed to a static vertical magnetic field of $B_0 \approx 1030$ nT, either pointing upwards or downwards, corresponding to a neutron Larmor precession frequency of $f_n = \frac{\gamma_n}{2\pi} B_0 \approx 30$ Hz. This highly homogeneous magnetic field ($\delta B/B \approx 10^{-3}$) is generated by a $\cos\theta$ coil. In addition, a set of trim coils permits the optimization of the magnetic field uniformity or the application of magnetic field gradients. These coils are wound on the outside of the cylindrical vacuum tank, which is surrounded by a four-layer mu-metal magnetic shield.

During the storage of polarized UCN, the Ramsey method of separated oscillatory fields is employed in order to measure f_n accurately. At the beginning of the storage period, a first oscillating horizontal field pulse of frequency $f_{RF} \approx f_n$ is applied for t = 2 s, thereby flipping the neutron spins by $\pi/2$. Next, the UCN spins are allowed to precess freely in the horizontal plane around the B_0 field, for a precession time of T = 180 s. A second $\pi/2$-pulse, at the same frequency f_{RF} and in phase with the first pulse, is then applied. The Ramsey procedure is resonant in the sense that it flips the neutron spins by exactly π only when $f_{RF} = f_n$.

In order to monitor the magnetic field B_0 within the precession chamber, a cohabiting mercury magnetometer is used [12]. A gas of ^{199}Hg mercury atoms is continuously polarized by optical pumping in a polarization chamber situated below the precession chamber. At the beginning of a measurement cycle, the precession chamber is filled with polarized atoms, and a $\pi/2$ mercury pulse is applied immediately before the first neutron pulse. Thus, during the precession time, both neutron spins and mercury spins precess in the horizontal plane, sampling the same volume. The Larmor frequency $f_{Hg} = \frac{\gamma_{Hg}}{2\pi} B_0 \approx 8$ Hz of the mercury atoms is measured by optical means: the modulation of the transmission of a circularly polarized resonant UV light beam from a ^{204}Hg discharge lamp is measured with a photomultiplier tube. For each cycle, the mercury comagnetometer provides a measurement of the magnetic field averaged

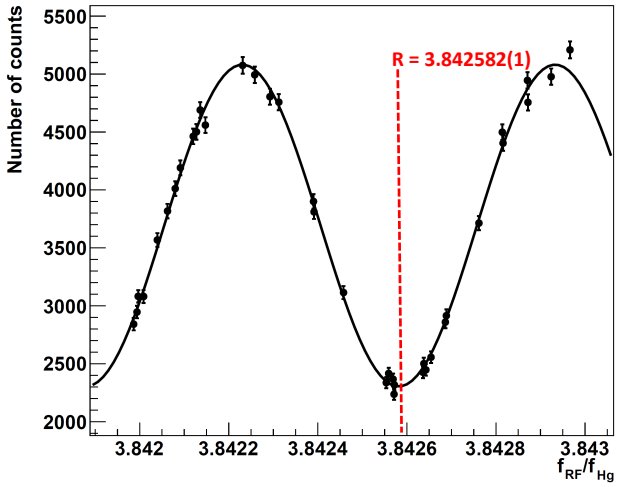


Figure 2: Ramsey fit for the run 6043. In this run the goodness-of-fit is quantified by $\chi^2/d.o.f. = 1.3$.

over the same period of time as for the neutrons, at an accuracy of $\sigma(f_{\rm Hg}) \approx 1\,\mu$Hz.

A typical run consists of a succession of $\sim$ 20 cycles, in which the neutron pulse frequency $f_{\rm RF}$ is randomly varied. We analyzed each run to extract the neutron to mercury frequency ratio $R = f_{\rm n}/f_{\rm Hg}$, which, in absence of systematic effects, would be equal to $\gamma_{\rm n}/\gamma_{\rm Hg}$. In a Ramsey experiment, the phase of the spin after the effective precession time $T + 4t/\pi$ is $\phi = 2\pi(f_{\rm RF} - f_{\rm n})(T + 4t/\pi)$ (see e.g. [13] for a derivation of the factor $4/\pi$). When the magnetic field acting on the neutron is monitored via the mercury precession frequency, then the analysis of a run consists in fitting a Ramsey fringe pattern to the data, according to

$$N_i^{\rm up} = N_0\left(1 - \alpha\cos(K(f_{\rm RF,i}/f_{{\rm Hg},i} - R))\right), \tag{3}$$

where $N_i^{\rm up}$ is the number of neutron counts in cycle i, $f_{\rm RF,i}$ is the frequency of the neutron $\pi/2$-pulses for cycle i and $f_{{\rm Hg},i}$ the measured mercury precession frequency. The parameter K defined by

$$K = 2\pi(T + 4t/\pi)\langle f_{\rm Hg}\rangle \tag{4}$$

represents the period of the fringes, where $\langle f_{\rm Hg}\rangle$ is the mean mercury frequency during the run. For each run the three parameters α (visibility of the Ramsey fringe), N_0 and R are extracted from the fit. An example of a run is shown in Fig. 2. The vertical error bars follow from counting statistics and the horizontal error bars are negligible. The sensitivity of the technique is thus limited by neutron counting statistics and was on average $\sigma(R) = 1.5 \times 10^{-6}$ per run.

Different runs correspond to different trim coil current settings and thus different magnetic field gradients. The measurements with different magnetic field configurations serve to correct the systematic effects described in the next section. For the sake of simplicity we have retained for the final analysis only runs with gradients smaller than 200 pT/cm, i.e. 7 runs with the magnetic field pointing downwards and 9 runs with the magnetic field pointing upwards.

3. Systematic effects

There are four known effects that could significantly shift the ratio $R = f_{\rm n}/f_{\rm Hg}$ from its unperturbed value $\gamma_{\rm n}/\gamma_{\rm Hg}$, either by affecting the neutron frequency or the mercury frequency. We write the combination of all these effects as

$$R = \frac{f_{\rm n}}{f_{\rm Hg}} = \frac{\gamma_{\rm n}}{\gamma_{\rm Hg}}\left(1 + \delta_{\rm Grav} + \delta_{\rm T} + \delta_{\rm Light} + \delta_{\rm Earth}\right), \tag{5}$$

and address them in detail in what follows.

The most important effect is known as the gravitational shift $\delta_{\rm Grav}$. The room temperature gas of mercury atoms fills the storage volume with a uniform density in all spatial directions. Conversely, the much colder UCN gas is strongly affected by gravity and the UCN density is significantly higher at the bottom of the storage chamber than at the top. This results in a difference h of the vertical locations of the centers of mass of the two species which, in turn, results in a shift of the ratio R in the presence of a vertical magnetic field gradient:

$$\delta_{\rm Grav}^{\uparrow/\downarrow} = \pm\frac{h}{B_0}\frac{\partial B}{\partial z}, \tag{6}$$

where the arrows and the $\pm$ sign refer to the direction of the magnetic field. A direct measurement of this effect was reported in [14].

To correct for the gravitational shift, the magnetic field gradient was measured using an array of cesium magnetometers (four magnetometers on the top of the chamber and seven on the bottom; see Fig. 1). The working principle of these magnetometers is described in [16]. The transverse components of the magnetic field are small, therefore the scalar magnetometers are effectively measuring the longitudinal component: $B \approx B_z$. For each run, a field value was extracted for each magnetometer by averaging the magnetometer readings over the duration of the run. A second-order parameterization of the field was then fitted to the field measured at the positions of the eleven magnetometers. The parameterization

$$\begin{aligned} B(x,y,z) = \; & b_0 + g_x x + g_y y + g_z z + g_{xx}(x^2 - z^2) + \\ & g_{yy}(y^2 - z^2) + g_{xy}xy + g_{xz}xz + g_{yz}yz, \end{aligned} \tag{7}$$

is the most general second order polynomial satisfying constraints imposed by Maxwell's equation. The nine parameters were extracted by performing an unweighted least-squares minimization. The main parameter of interest is g_z, since the differences of the UCN and mercury volume averages for the other terms are negligible. For an error evaluation on g_z, the jackknife procedure was applied, by removing one magnetometer at a time and performing the fit always with ten magnetic field values. The standard deviation of those eleven values for g_z was then used as the uncertainty on g_z. The jackknife error obtained by this procedure was 8 pT/cm. This analysis method was tested using toy data [15], it was found that the jackknife procedure accounts for the incompleteness of the second order parametrization (7) and for the possible offsets of the magnetometers.

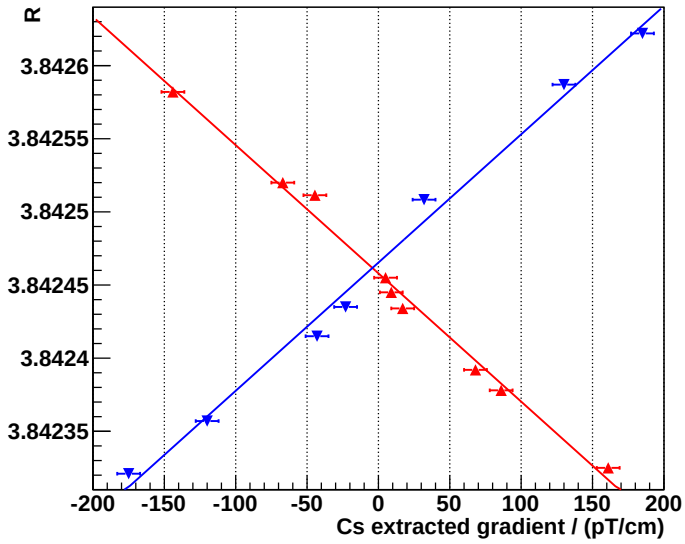


Figure 3: Neutron to mercury frequency $R = f_n/f_{Hg}$ plotted as a function of the field gradient. Upwards-pointing (red) and downwards-pointing (blue) triangles represents runs in which B_0 was pointing upwards and downwards, respectively. The vertical error bars are smaller than the size of the triangles.

Figure 3 shows the R value for each run as a function of the gradient g_z. We extrapolate the R value to the limit of vanishing gradient by performing a combined fit of the data according to

$$R^{\uparrow} = R_0^{\uparrow}\left(1 + \frac{h}{B_0} g_z^{\uparrow}\right) \quad \text{and} \quad R^{\downarrow} = R_0^{\downarrow}\left(1 - \frac{h}{B_0} g_z^{\downarrow}\right), \tag{8}$$

and obtain the following values for the three fit parameters:

$$h = -0.235(5)\,\text{cm}, \tag{9}$$
$$R_0^{\uparrow} = 3.8424580(23), \tag{10}$$
$$R_0^{\downarrow} = 3.8424653(27). \tag{11}$$

The goodness-of-fit is quantified by $\chi^2/\text{d.o.f} = 23/13$, which supports the validity of the gradient errors. An analysis of an extended set of data, including runs with higher magnetic field gradients, has been performed independently [17], confirming the result presented here. The values $R_0^{\uparrow}$ and $R_0^{\downarrow}$ are intermediate quantities for which Eq. (5) holds with the δ_{Grav} term set to zero. The other three systematic effects, which depend solely at first order on the magnetic field direction, still need to be corrected.

The second systematic effect δ_T arises from residual transverse magnetic field components B_T. The neutron magnetometer is sensitive to the volume average of the magnetic field modulus, viz. $f_n \propto \langle|\vec{B}|\rangle$ since the neutron Larmor frequency is larger than the wall collision frequency (adiabatic regime). On the other hand, the mercury Larmor frequency is much lower than the wall collision frequency. As a consequence the mercury magnetometer is sensitive to the vectorial volume average of the field: $f_{Hg} \propto |\langle\vec{B}\rangle|$. From this essential difference the resulting frequency shift due to a transverse field is given by

$$\delta_T = \frac{\langle {B_T}^2\rangle}{2B_0^2}, \tag{12}$$

where $\langle {B_T}^2\rangle$ is the volume average over the precession chamber of the squared transverse field.

To correct for the transverse shift we performed an extensive magnetic-field mapping of the precession chamber region using a three-axis fluxgate magnetometer attached to a robot mapper. From the magnetic-field maps we were able to extract the transverse field components in both configurations B_0 up and B_0 down:

$$\langle {B_T}^2\rangle^{\uparrow} = (2.1 \pm 0.5)\,\text{nT}^2 \;;\; \langle {B_T}^2\rangle^{\downarrow} = (1.7 \pm 0.7)\,\text{nT}^2. \tag{13}$$

From this we infer corrections given by

$$\delta_T^{\uparrow} = (1.0 \pm 0.2) \times 10^{-6} \;;\; \delta_T^{\downarrow} = (0.8 \pm 0.3) \times 10^{-6}. \tag{14}$$

The third systematic effect δ_{Light} arises from a possible light shift of the mercury precession frequency induced by the light beam that detects the Hg free-induction decay. This phenomenon, discovered in 1961 by Cohen-Tannoudji [18], is a shift of the resonance frequency proportional to the UV light intensity. We performed a dedicated test to quantify this effect, by measuring the mercury frequency while varying the light intensity. The light shift has a vectorial component, i.e. it could depend on the angle between the light beam axis and the magnetic field direction. Therefore the associated frequency shift could in principle depend on the B_0 direction. We performed the test for both B_0 polarities and we report the result:

$$\delta_{\text{Light}}^{\uparrow} = (0.34{\pm}0.18){\times}10^{-6} \;;\; \delta_{\text{Light}}^{\downarrow} = (0.21{\pm}0.14){\times}10^{-6}. \tag{15}$$

The last systematic effect δ_{Earth} is a shift due to the Earth's rotation (see [19] for a discussion of this effect in the context of the nEDM). The precession frequencies of the neutron and the mercury results from the Larmor frequencies in a non-rotating frame combined with the rotation of the Earth. One can derive the following expression for the associated frequency shift

$$\delta_{\text{Earth}}^{\uparrow/\downarrow} = \mp\left(\frac{f_{\text{Earth}}}{f_n} + \frac{f_{\text{Earth}}}{f_{Hg}}\right)\sin(\lambda) = \mp 1.4 \times 10^{-6}, \tag{16}$$

where $f_{\text{Earth}} = 11.6\,\mu\text{Hz}$ is the Earth's rotation frequency and $\sin(\lambda) = 0.738$ the sine of the latitude of the PSI location. The conventions are such that f_n and f_{Hg} are positive frequencies. In the derivation of Eq. (16) it was important to consider that the true neutron and mercury gyromagnetic ratios are negative and positive quantities, respectively.

The relative difference between the R ratios measured with B_0 up and B_0 down, after correcting for the gravitational, transverse, and light shifts, should amount to the Earth's rotation effect, whose anticipated value is $\delta_{\text{Earth}}^{\uparrow} - \delta_{\text{Earth}}^{\downarrow} = -2.7 \times 10^{-6}$. Indeed we find

$$2\frac{R_0^{\uparrow} - R_0^{\downarrow}}{R_0^{\uparrow} + R_0^{\downarrow}} - (\delta_T^{\uparrow} - \delta_T^{\downarrow}) - (\delta_{\text{Light}}^{\uparrow} - \delta_{\text{Light}}^{\downarrow}) = (-2.2{\pm}1.0){\times}10^{-6}, \tag{17}$$

in agreement with the expected value.

Table 1: Error budget for the measurement of γ_n/γ_{Hg}

Effect	$B_0 \uparrow$	$B_0 \downarrow$
Counting statistics	$\pm 0.5 \times 10^{-6}$	$\pm 0.5 \times 10^{-6}$
Gravitational shift $(3.84 \times \delta_{Grav})$	$(-8.9 \pm 2.3) \times 10^{-6}$	$(-1.8 \pm 2.7) \times 10^{-6}$
Intermediate R_0	3.8424580(23)	3.8424653(27)
Transverse shift $(3.84 \times \delta_T)$	$(3.7 \pm 0.8) \times 10^{-6}$	$(3.0 \pm 1.2) \times 10^{-6}$
Light shift $(3.84 \times \delta_{Light})$	$(1.3 \pm 0.7) \times 10^{-6}$	$(0.8 \pm 0.6) \times 10^{-6}$
Earth rotation $(3.84 \times \delta_{Earth})$	-5.3×10^{-6}	$+5.3 \times 10^{-6}$
Corrected value	3.8424583(26)	3.8424562(30)
Combined final γ_n/γ_{Hg}	3.8424574(30)	

Table 2: Key data for each run selected for the analysis: the fitted visibility α, the ratio R, the average field B_{Hg} extracted from the mercury comagnetometer, the gradient g_z extracted from the Cs magnetometer array and the squared transverse field $\langle {B_T}^2 \rangle$ extracted from the field maps are reported.

Run #	α	R	B_{Hg} [nT]	g_z [pT/cm]	$\langle {B_T}^2 \rangle$ [nT^2]
		$B_0 \downarrow$			
6015	0.41	3.842321	1031.86	-175	2.5
6016	0.48	3.842587	1031.33	130	1.8
6023	0.66	3.842435	1031.60	-23	1.1
6027-8	0.57	3.842508	1030.18	32	1.0
6030	0.55	3.842415	1030.32	-43	1.0
6031	0.38	3.842622	1029.92	185	2.6
6033	0.48	3.842357	1030.45	-120	1.7
		$B_0 \uparrow$			
6040-1	0.54	3.842445	1027.97	9	1.7
6042	0.36	3.842325	1028.23	161	2.6
6043	0.38	3.842582	1027.70	-144	3.0
6047	0.46	3.842520	1027.82	-67	2.1
6049	0.43	3.842378	1028.14	86	1.9
6058	0.53	3.842434	1027.82	17	1.7
6059	0.42	3.842511	1026.82	-44	2.0
6060	0.55	3.842455	1028.25	5	1.7
6064	0.44	3.842392	1029.47	68	1.9

Two additional minor systematic effects were considered and neglected. First, the Bloch-Siegert shift of the neutron resonance, associated with the use of a linearly oscillating rather than rotating field for applying the $\pi/2$-pulses, is calculated to be 2 µHz. Second, possible biases induced by the DAQ electronics were investigated. A dedicated multifunction electronic module [20] synchronized on an atomic clock serves both to generate the neutron pulses and to sample the mercury precession signal. We checked that effects that could modify the frequency ratio, such as a loss of phase coherence between the two neutron pulses, are negligible.

The error budget and the correction procedure are summarized in Table 1 and the key data for each run is presented in Table 2. As a final step we combine the results obtained for B_0 up and B_0 down. The agreement between these two results provides a nontrivial consistency check. To avoid double use of data, we conservatively quote for the final uncertainty the

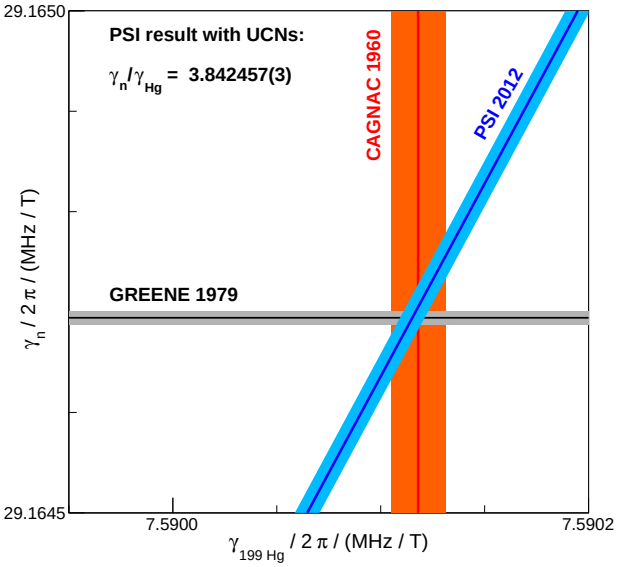


Figure 4: 1-sigma allowed regions in the γ_n, γ_{Hg} plane. Our final value for the neutron to mercury magnetic moment ratio (18) here labeled as "PSI 2012" forms the diagonal band. The horizontal band is the neutron magnetic moment (1) value from Greene et al. and the vertical band is from the measurement of the mercury magnetic moment (2) by Cagnac.

largest of the two individual errors:

$$\gamma_n/\gamma_{Hg} = 3.8424574(30) \quad [0.78\,\text{ppm}]. \tag{18}$$

4. Discussion

Our result (18) can be considered as a consistency check of the accepted values for the neutron and ^{199}Hg magnetic moments as shown in Fig. 4. Equivalently, this result provides a new accurate and independent measurement of the neutron gyromagnetic ratio. Using (2), we obtain:

$$\frac{\gamma_n}{2\pi} = 29.164705(55)\,\text{MHz/T} \quad [1.89\,\text{ppm}], \tag{19}$$

thus confirming the accepted value which, until now, was based on a single measurement [6].

Alternatively, we can use the results (1) and (18) to propose a new, more accurate value of the ^{199}Hg atomic gyromagnetic ratio:

$$\frac{\gamma_{Hg}}{2\pi} = 7.5901152(62)\,\text{MHz/T} \quad [0.82\,\text{ppm}]. \tag{20}$$

Acknowledgments

We are grateful to the PSI staff (the accelerator operating team and the BSQ group) for providing excellent running conditions and acknowledge the outstanding support of M. Meier and F. Burri. Support by the Swiss National Science Foundation Projects 200020-144473, 200021-126562, 200020-149211 (PSI) and 200020-140421 (Fribourg) is gratefully acknowledged. The LPC Caen and the LPSC acknowledge the support

of the French Agence Nationale de la Recherche (ANR) under reference ANR-09–BLAN-0046. Polish partners want to acknowledge The National Science Centre, Poland, for the grant No. UMO-2012/04/M/ST2/00556. This work was partly supported by the Fund for Scientific Research Flanders (FWO), and Project GOA/2010/10 of the KU Leuven. The original apparatus was funded by grants from the UKs PPARC.

References

[1] L. W. Alvarez and F. Bloch, Phys. Rev. **57** (1940) 111.
[2] W. R. Arnold and A. Roberts, Phys. Rev. **71** (1947) 878.
[3] F. Bloch, D. B. Nicodemus and H. H. Staub, Phys. Rev. **74** (1948) 1025.
[4] V. W. Cohen, N. R. Corngold and N. F. Ramsey, Phys. Rev. **104** (1956) 283.
[5] G. L. Greene *et al.*, Phys. Rev. D **20** (1979) 2139.
[6] P. J. Mohr, B. N. Taylor and D. B. Newell, Rev. Mod. Phys. **84** (2012) 1527.
[7] C. A. Baker *et al.*, Physics Procedia **17**, (2011) 159.
[8] B. Cagnac, Ann. Phys. **6** (1961) 467.
[9] C. A. Baker *et al.*, Phys. Rev. Lett. **97**, (2006) 131801.
[10] C. A. Baker *et al.*, Nucl. Instrum. Methods A **736**, (2014) 184.
[11] A. Anghel *et al.*, Nucl. Instrum. Methods A **611**, (2009) 272.
B. Lauss, Physics Procedia **51**, (2014) 98.
[12] K. Green *et al.*, Nucl. Instrum. Methods A **404**, (1998) 381.
[13] F. M. Piegsa *et al.*, Nucl. Instrum. Methods A **589**, (2008) 318.
[14] I. Altarev *et al.*, Physica B **406** (2011) 2365.
[15] V. Helaine, PhD thesis, Caen University (2014).
[16] P. Knowles *et al.*, Nucl. Instrum. Methods A **611** (2009) 606.
[17] B. Franke, PhD thesis no. 21562, ETH Zuerich (2013).
[18] C. Cohen-Tannoudji, C. R. Acad. Sci. **252** (1961) 394.
[19] S. K. Lamoreaux and R. Golub, Phys. Rev. Lett. **98** (2007) 149101.
[20] O. Bourrion *et al.*, Nucl. Instrum. Methods A **701** (2013) 278.